Effects of the electric current on the superplastic behavior of 3Y-TZP in oxygen-lean atmosphere.

Kang Wang , Yufei Zu , Guoqing Chen * , Xuesong Fu , Wenlong Zhou

Posted Date: 20 July 2023

doi: 10.20944/preprints202307.1382.v1

Keywords: 3Y-TZP ceramic; electric current; superplastic deformation; electrochemical reduction reaction

Article

Effects of the Electric Current on the Superplastic Behavior of 3Y-TZP in Oxygen-Lean Atmosphere

Kang Wang [1], Yufei Zu [2] GuoqingChen [1,*],XuesongFu [1] and WenlongZhou [1]

[1] Key Laboratory of Solidification Control and Digital Preparation Technology (Liaoning Province), School of Materials Science and Technology, Dalian University of Technology, Dalian 116085, China
[2] Key Laboratory of Advanced Technology for Aerospace Vehicles (Liaoning Province), School of Aeronautics and Astronautics, Dalian University of Technology, Dalian 116085, China
* Correspondence: gqchen@dlut.edu.cn; Tel: +0411-84707970

Abstract: The superplastic behavior of 3Y-TZP with the electric currents in oxygen-lean atmosphere were investigated. the superplastic deformation of 3Y-TZP can be promoted by the electric current at a strain rate of 6.67 × 10−4 s^{-1} and a furnace temperature of 1200 °C. The stress exponent n within 2~3 indicated that the mechanism for the deformation was the grain boundary sliding accompanied by diffusion. The applied electric current decreased the apparent activation energy Q of the deformation from 465 kJ mol^{-1} to 315 kJ mol^{-1}, resulting in a transition of the diffusion mechanism from the lattice diffusion to the grain boundary diffusion. In addition, the remarkable variation of the electric property and grain growth demonstrated that these phenomena were mainly attributed to the enhancement of the cation diffusion caused by the electrochemical reduction reaction, which induced by the electric current in oxygen-lean atmosphere.

Keywords: 3Y-TZP ceramic; electric current; superplastic deformation; electrochemical reduction reaction

1. Introduction

Structural ceramics are attractive because of their excellent mechanical properties, such as high hardness, high strength and low density. What they lack, however, is fracture toughness and machinability to a desired shape. In recent years, some structure ceramics with grain sizes less than 1 μm exhibited superplasticity [1–7], which the tensile elongation exceeded 100% through the grain boundary sliding (GBS). Hence, superplastic forming is expected to be an effective way for fabricating ceramic components having complex shapes.

Following the initial report by Wakai et al. [1,3,8]of a great elongation of 170% in yttria-stabilized tetragonal zirconia (TZP), there had been a considerable amount of research activity on the superplastic ceramics. Morita et al. [9] doped 30% spinel in zirconia at 1550 ℃ to obtain an elongation of 660%. Yoshida et al. [10] reported the tensile deformation of TZP doped with TiO_2-GeO_2, which exhibited a largest elongation of 1053% at 1400°C. Recently, the electric field, reported by some studies, was used for improving the plastic deformation of the structural ceramics. At different electric fields field, work by Conrad and co-workers [11–16] on yttria-stabilized tetragonal zirconia in air showed a significant enhancement in ductility. They also discovered that the flow stress with the electric field can be decreased by retarding the grain growth. However, all these experiments were operated at temperatures above 1400 ℃ and strain rates below 10^{-4} s^{-1}, which would make it difficult to achieve the industrial production of structural ceramics.

More recently, Raj and coworkers [17] reported that the sintering of yttria-stabilized zirconia can be densified rapidly in a few seconds with a high DC electric fields (100 Vcm^{-1}) at low furnace temperatures (<1000 ℃). They believed that the applied electric field on yttria-stabilized zirconia may accelerate the diffusional transport during the sintering. However, Luo and coworkers [18] discovered that a reduced atmosphere can effectively promote the flash sintering of ZnO to achieve nearly full densities at furnace temperature below 120 °C. In addition, Hulbert et al. [19] also discovered that a high-strain-rate formable in ZrO_2-Al_2O_3-spinel composite ceramics can be achieved by using spark plasma sintering (SPS) equipment at a furnace temperature of 1100 °C. They believed that this high-speed superplastic forming was made possible by taking advantage of the enhanced

Preprints (www.preprints.org) | NOT PEER-REVIEWED | Posted: 20 July 2023 doi:10.20944/preprints202307.1382.v1

diffusional transport in the SPS chamber environment. Dong and Chen [20,21] reported that grain growth in zirconia can be accelerated in N_2 + 5%H_2 atmosphere by an electric current. They pointed out that this remarkable grain growth was related to the enhancement of cation diffusion in an oxygen-lean atmosphere. Therefore, an oxygen-lean atmosphere will inevitably affect the deformation behavior and mechanism of the electric field/current assisted superplastic deformation on zirconia.

It is well known that the deformation behavior and the corresponding mechanism for structure ceramics can be identified by the following constitutive equation:

$$\dot{\varepsilon} = A\sigma^n d^{-p} \exp\left(-\frac{Q}{RT}\right) \quad (1)$$

where A is a constant, $\dot{\varepsilon}$ is the steady state strain rate, σ is the applied stress, d is the average grain size, n is termed the stress exponent, the parameter p is the grain size exponents, and the Q, R and T are the activation energy, gas constant, and absolute temperature, respectively.

Wakai.F et al. [1,8,22,23] investigated the superplastic behavior of ZrO_2 polycrystals without the electric field, and the corresponding mechanism for the deformation was grain boundary sliding accompanied by diffusion. Meanwhile, more reports on the deformation characteristics of yttria-stabilized tetragonal zirconia also indicated that the dominant mode of the deformation for yttria-stabilized tetragonal zirconia was grain boundary sliding, and the stress exponent had a change from n=2 in high stress region to n=3 in low stress region [24]. Hines et al. [25] agreed with these views and demonstrated that the transition in stress exponents could be explained by two sequential mechanisms: interface reaction controlled by grain boundary sliding (n=3) and grain boundary sliding (n=2), respectively. Moreover, for yttria-stabilized tetragonal zirconia (3Y-TZP), Conrad and co-workers [12] reported that the of the stress exponent n of the deformation with field was the same as without. which indicated that the dominant mode of the deformation for 3Y-TZP was not altered by the electric field. However, there are few research concerned the behavior and mechanism of the electric field assisted plastic deformation on zirconia ceramic in an oxygen-lean atmosphere.

Therefore, the present work aims to investigate the mechanism of the electric current assisted plastic deformation on 3Y-TZP in oxygen-lean atmosphere. For this purpose, the flow behavior of 3Y-TZP was examined at the different initial strain rates and temperatures.

2. Experimental Procedures

The starting materials used in this paper were powders of TZ-3Y, with a particle size of 27 nm (Tosoh Co. Tokyo, Japan). The composition in weight percent was Y_2O_3=5.15%, Al_2O_3=0.005%, SiO_2=0.003%, Fe_2O_3=0.003% and Na_2O=0.021%. The specimens for the deformation were sintered by using this powders at 1200 °C, 30 MPa applied pressure and 1 hour holding time in a Hot Press Sintering Furnace. The relative density of the as-sintered specimen was 99.3%, which measured by the Archimedes method. The geometry of the as-sintered 3Y-TZP for the compression deformation was cylindrical, with 10 mm in diameter and 10 mm in height. The SEM micrographs of the as-sintered 3Y-TZP specimen was shown in Figure 1.

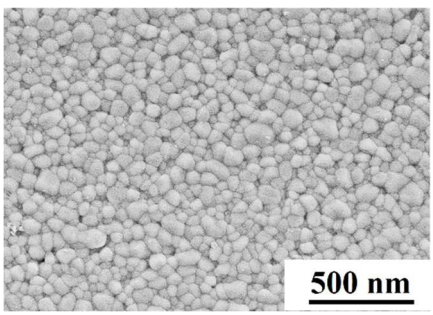

Figure 1. The microstructure of sintered zirconia at 1200 ℃.

The deformation experiment was operated by the self-designed equipment. In order to ensure the electric current only passes though the specimen, the special graphite with an alumina tube wan designed. The upper/lower graphite indenter was connected with a voltage stabilized DC power

Preprints (www.preprints.org) | NOT PEER-REVIEWED | Posted: 20 July 2023 doi:10.20944/preprints202307.1382.v1

supply device by using electric wires. The deformation temperatures were set to 1200 °C, 1300 °C, and 1400 °C, and the furnace was heated at a rate of 10°C·min^{-1} until reached the set temperature. In order to guaranteeing a uniform temperature, the specimens were kept at the deformation temperature for 10 min before the deformation. A platinum-rhodium thermocouple was used to measure the furnace temperature. The experiment was operated at different electric currents: 1 A, 3 A, and 5 A. For each applied electric current, the immediate height H_x and the load P were recorded by adjusting the punch rates at 0.1, 0.2 and 0.4 mm·min^{-1}, respectively. The initial end face area A_0 and the initial height H_0 of the cylindrical specimen are directly measured. The strain rate $\dot{\varepsilon}$, the true stress σ, and the true compressive strain ε of the specimens were expressed as the follow equations:

$$\dot{\varepsilon} = \frac{H_x - H_{x-1}}{H_x} \tag{2}$$

$$\sigma = \frac{PH_x}{A_0 H_0} \tag{3}$$

$$\varepsilon = -\ln\left(\frac{H_x}{H_0}\right) \tag{4}$$

The specimens were polished by a diamond paste of 1.5 μm in diameter and thermally etched for 100 min at a temperature 50 °C lower than the sintering and/or deformation temperatures in oxygen atmosphere. The microstructures of the specimen were characterized by a scanning electron microscopy (SEM) system (S-4300, Hitachi, Japan). The average grain sizes of the deformed specimens were calculated by using the linear intercept method. The relative amounts of the oxygen vacancy were calculated by the X-ray photoelectron spectroscopy, which obtained from the X-ray photoelectron spectrometer (Kratos, ultra^{DLD}, UK).

3. Results and discussion

The stress-strain curves of 3Y-TZP specimens with and without the electric current are shown in Figure 2.

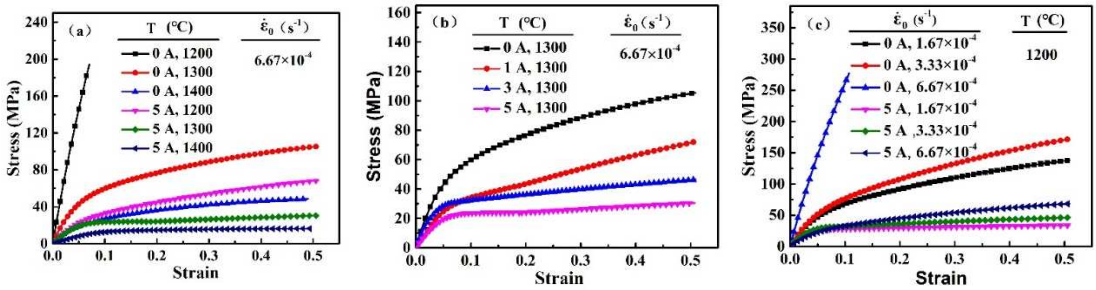

Figure 2. the true stress–strain date of 3Y-TZP with and without the electric currents at the different furnace temperatures and initial deformation rates.

Evident in Figure 2 is that the electric current can effectively decrease the flow stress during superplastic deformation of 3Y-TZP. For example, The Figure 2(a) showed that the 3Y-TZP specimen at an initial strain rate of $\dot{\varepsilon}_0 = 6.67 \times 10^{-4}$ s^{-1} without the electric current exhibited a limited plastic strain and high stress (268 MPa) at 1200 °C, compared to that at 1400 °C (48.52 MPa). By contrast, as the electric current applied, the flow stress of deformation decreased sharply. The flow stress of the specimen with the electric current (I= 5A) at 1200 °C was only 63.59 MPa. The flow stress decreases during the deformation as the electric current increases (Figure 2(b)). In addition, the deformation of 3Y-TZP at different initial deformation rates can also be promoted by the electric current(Fig. 2(c)). These results indicated that the electric current was instrumental in decreasing the flow stress and the furnace temperature during the superplastic deformation of 3Y-TZP in oxygen-lean atmosphere.

The microstructures of the deformed 3Y-TZP at cross-section, which parallel to the compression direction, are show in Figure 3.

Preprints (www.preprints.org) | NOT PEER-REVIEWED | Posted: 20 July 2023 doi:10.20944/preprints202307.1382.v1

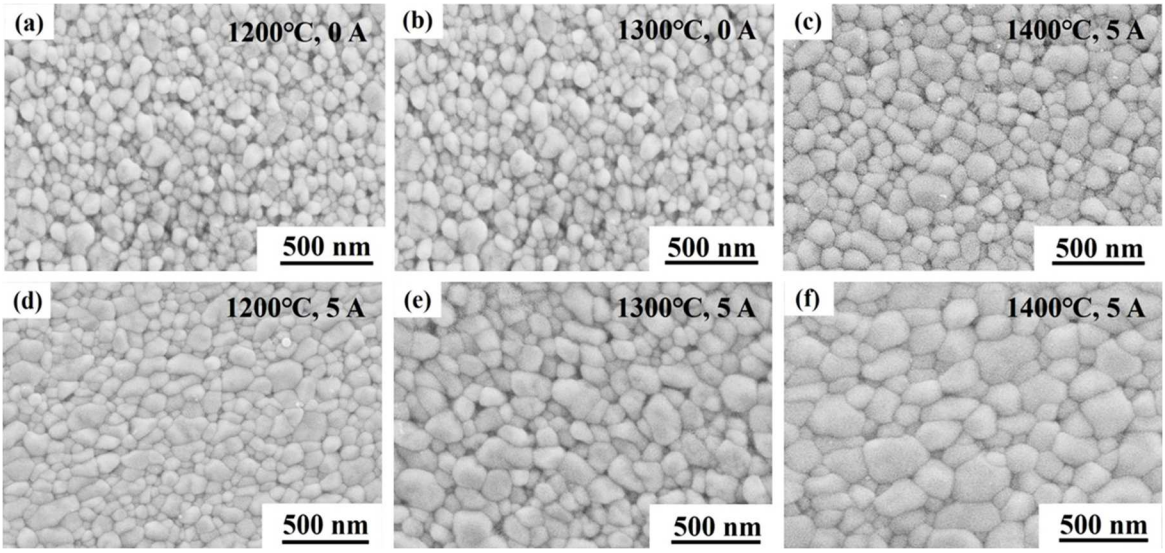

Figure 3. Microstructures of the deformed 3Y-TZP with/without the electric current at different furnace temperatures: (a) 0A, 1200 ℃, (b) 0A, 1300 ℃, (c) 0A, 1400 ℃, (d) 5A, 1200 ℃(e)5A, 1300 ℃(f) 5A, 1400 ℃. Average grain sizes: (a) 121 nm, (b) 138 nm, (c) 168 nm, (d) 163 nm, (e) 262 nm, (f) 359 nm.

It is clearly that all deformed specimens exhibited uniform microstructures with equiaxed grains, which the electric current had no effect on the grain aspect during deformation. Noteworthy is the pronounced difference in the average grain sizes. Upon applying the electric currents, a notable grain growth was promoted in the specimens during the deformation. The average grain size of the deformed specimen with 5 A at 1200 ℃, 1300 ℃ and 1400 ℃ were achieved 163 nm, 262 nm and 359 nm, respectively, which were larger than that without the electric current. This phenomenon was different from that reported by Conrad and coworkers [26]. They found that the grain growth in 3Y-TZP can be suppressed by the electric field during the superplastic deformation in air. Thus, the rapid grain growth in present experiment was related to the oxygen-lean atmosphere. Recent studies by Chen and coworkers[20] demonstrated that the application of an electric current to 3YSZ was effective in promoting grain growth during heat treatment in the N_2 + 5%H_2 atmosphere. And this grain growth caused by the electric current was closely related to the enhanced cation diffusion in oxygen-lean atmosphere. In addition, according to the black body radiation mode [27], the temperature of the specimen with 5 A at the furnace temperature of 1200 °C was only 1266 °C. The corresponding average grain size (Figure 3(d)) was obviously larger than that of the deformed specimen without electric current at 1300 °C (Figure 3(b)). these results indicated that this remarkable grain growth during the deformation was attributed to a mechanism of the cation diffusion enhanced by the electric current, apart from temperature rise. And this enhancement of the cation diffusion will inevitably affect the deformation mechanism.

The deformation mechanism is usually characterized by the stress exponent and microstructure. And the stress exponents (n) are obtained by the deformation experiments with an initial grain size of 0.11μm at the various initial strain rates. The relationships between the strain rate and flow stress with/without electric current are plotted on a logarithmic scale in Figure 4.

Preprints (www.preprints.org) | NOT PEER-REVIEWED | Posted: 20 July 2023 doi:10.20944/preprints202307.1382.v1

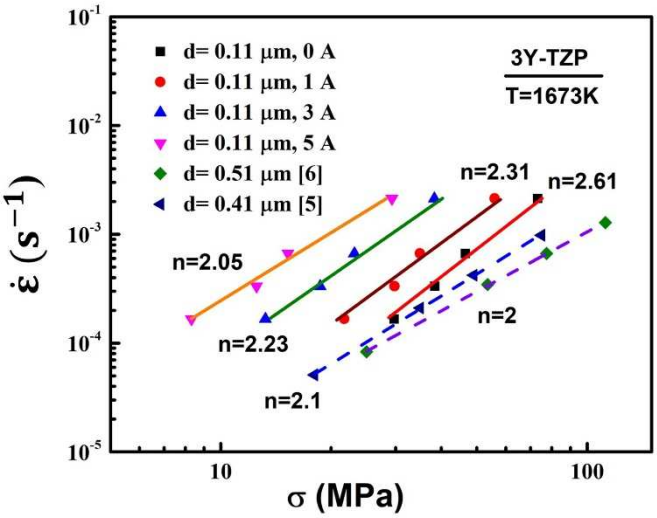

Figure 4. Variation of $\dot{\varepsilon}$ with σ on a logarithmic scale for specimens with the initial grain size d = 0.11 μmm deformed under the electric currents of 0A, 1A, 3A and 5A at temperature of 1400°C showing a change in n from 2.61 to 2.05.

As shown in Figure 4, the strain rate increased with a constant stress, with the electric current increased. The stress exponent of the specimens with the different electric currents at 1400 °C were 2.31, 2.23 and 2.05, respectively. The stress exponent of the specimens without electric current was 2.61. It is obvious that the value of the tress exponent n has a significant change while the electric current varies. As the electric current increases, the tress exponent n shows a continuous decreasing trend. According to the literature, the corresponding deformation mechanism were the superposition of grain boundary slip and diffusion creep (grain boundary sliding accompanied by diffusion) while the stress exponent n was between 2 and 3 [25]. Comparing with the microstructures, the strain rate in current-assisted deformation with a larger grain size was higher than that without the electric current. Thus, the higher strain rate with the electric current was is inevitably influenced by other factors except the grain size. These factors are usually the grain boundary structure/chemistry, the enhancement of diffusion, in particular, the diffusion enhancement via excess vacancy. In addition, According to Equation (1), for a given combination of the grain size, strain rate and temperature, the flow stress is determined by the diffusion mechanism, which is characterized by the apparent activation energy Q. Therefore, the electric current did not alter the major deformation mode of 3Y-TZP (grain boundary sliding). The lower flow stress in present study with the applied electric current had a faster diffusion. And The variation of the stress exponent n may be related to the enhancement of diffusion process induced by the electric current.

The diffusion mechanism of the deformation is always explained in terms of the lattice diffusion or the grain boundary diffusion. The relationship between temperatures and strain rates were shown in Figure 5.

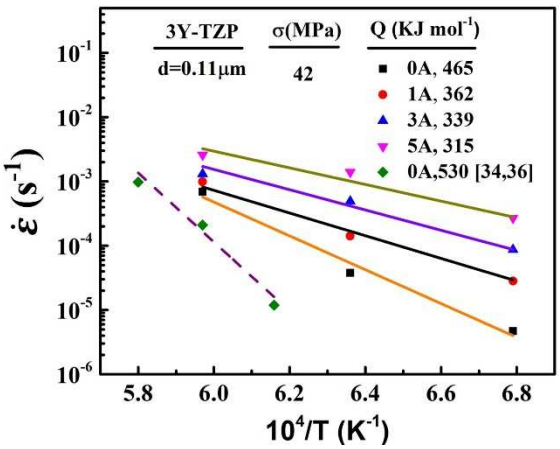

Preprints (www.preprints.org) | NOT PEER-REVIEWED | Posted: 20 July 2023 doi:10.20944/preprints202307.1382.v1

Figure 5. The effect of the temperature on the strain rate at 42 MPa.

The apparent activation energies were calculated for the electric currents of 0A, 1A, 3A and 5A as 465, 362, 339 and 315 kJ mol^{-1}, respectively. It can be clearly that the apparent activation energy decreased as the electric current increased. As mentioned by previous studies[29–31], the activation energies Q for grain boundary diffusion and lattice diffusion of Zr^{4+} cation in 3Y-TZP were around 370 kJ mol^{-1} and 530 kJ mol^{-1}, respectively [4,30]. Zapata et al[4] also found that the apparent activation energies Q in 3Y-TZP were independent of grain size. These results indicated that the accommodation process for superplastic flow on 3Y-TZP without electric current was the lattice diffusion (465kJ mol^{-1}). And the applied electric current can transform the lattice diffusion into grain boundary diffusion.

Generally, the cation diffusion, regarded as the rate-controlling species for the superplastic deformation in Y-TZP, had an important effect on this diffusion process [28] . And the cation diffusion in oxide ceramics can be promoted by the increase of point defects, which can also increase the diffusion rate. In air, the defect changed of 3YSZ can be expressed by the following equation [32]:

$$O_o^x = V_o^{\cdot\cdot} + 2e' + \frac{1}{2}O_{2(g)} \tag{5}$$

where $V_o^{\cdot\cdot}$ is the oxygen vacancies, O_o^x is the lattice oxygen, $O_{2(g)}$ is the molecular oxygen, e' is the free electron.

The concentration of O_o^x is assumed to be constant, which is insignificantly affected by the deviations of stoichiometry. The corresponding mass-action expression is expressed:

$$K = [V_o^{\cdot\cdot}][e']^2 P_{O_2}^{1/2} \tag{6}$$

where K is a constant, P_{O_2} is the oxygen partial pressure and the [] notation indicates concentration. Therefore, in oxygen-rich environments, the decrease P_{O_2} in will lead to an increase in the defect change of 3YSZ. If in an oxygen-lean atmosphere, an electrochemical reduction reaction will be occurred during the deformation [33].

$$\delta V_o^{\cdot\cdot} + ZrO_2 + 2\delta e' \rightarrow ZrO_{2-\delta} + \delta O_o^x \tag{7}$$

In this reaction, the oxygen ions remove from the 3Y-TZP lattice to form oxygen molecules. Correspondingly, the oxygen vacancies are incorporated into the 3Y-TZP lattice. In order to maintaining this oxygen vacancies will capture the electrons as a result of the charge balance, which will cause the specimen having a conversion from ZrO_2 into $ZrO_{2-\delta}$ [33–35] . The sketch summarizing the main electrochemical reaction is shown in Figure 6.

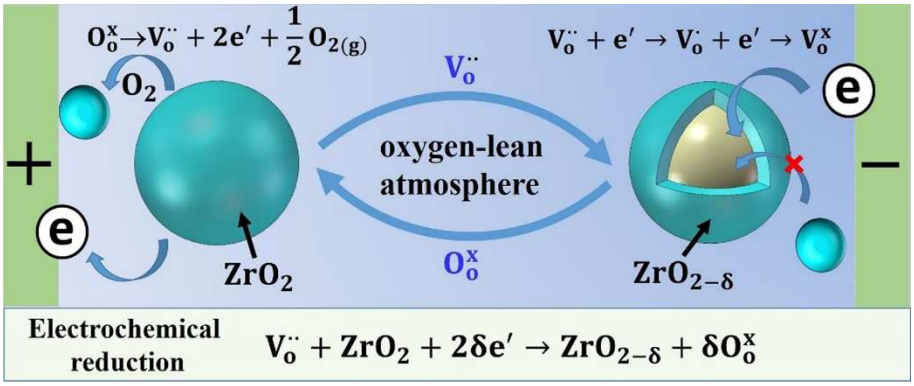

Figure 6. A schematic of electrochemical reduction reaction in 3Y-TZP subjected to the current assisted deformation.

As the reaction proceeds, a large amount of the oxygen vacancies will inevitably be generated in the specimen, and more electrons are enriched in the specimen. This extra oxygen vacancies generated by this reduction reaction can effectively promote the cation diffusion. Yoshida et al. [36] also believed that the lower flow stress and faster grain growth during the electric field assisted superplastic deformation of TZP were mainly attributed to the significantly accelerated diffusional

Preprints (www.preprints.org) | NOT PEER-REVIEWED | Posted: 20 July 2023 doi:10.20944/preprints202307.1382.v1

mass transport, which induced by the extrinsic oxygen anion vacancies that generated in reduced Y_2O_3-stabilized ZrO_2.

The relative amounts of the oxygen vacancy in the deformed specimens are detected by the X-ray photoelectron spectrometer, and the O 1s XPS spectrrum with 0 and 5 A of the deformed specimens at 1400°C are shown in Figure 7.

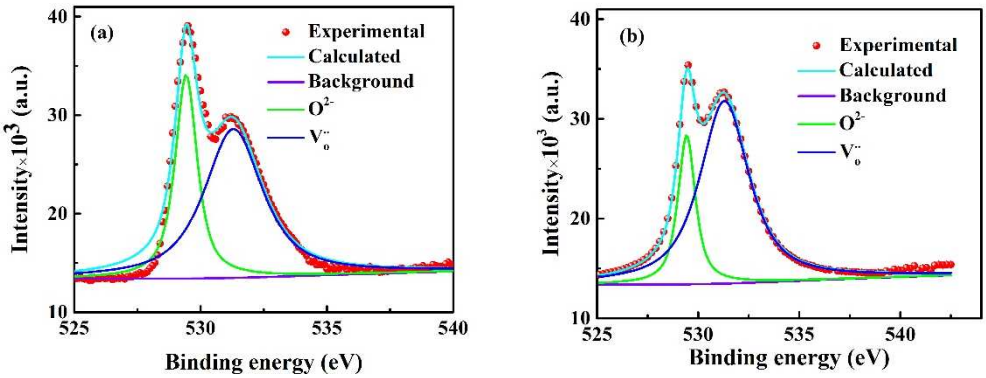

Figure 7. High-resolution O 1s XPS spectrum of the deformed samples: (a) 0 A, (b) 5 A.

The XPS spectrum of O 1s with 5 A (Figure 7 (b) can resolve into the different peaks centered at 531.0 eV and 529.2 eV by the deconvolution on spectrum. These different peaks conformed to the non-lattice oxygen (oxygen vacancy) and lattice oxygen, respectively. The relative amount of the oxygen vacancies is 79.1% in the deformed region with 5 A while 65.3% for that without the electrical current, which calculated by the corresponding peak area. Obviously, the oxygen vacancies in the deformed specimens were higher than that without the electric current. Meanwhile, Apurba et al [37] also found that the oxygen vacancy in the $ZrO_{2-\delta}$ was much higher than ZrO_2. Thus, these extra oxygen vacancies generated in present experiment were mainly attributed to the electrochemical reduction reaction induced by the electric current.

Figure 8 provides another evidence for the electrochemical reduction reaction. As shown in Figure 8, it is clearly that the different electric current produced different initial voltages, and the initial voltages decreases as the deformation proceeds.

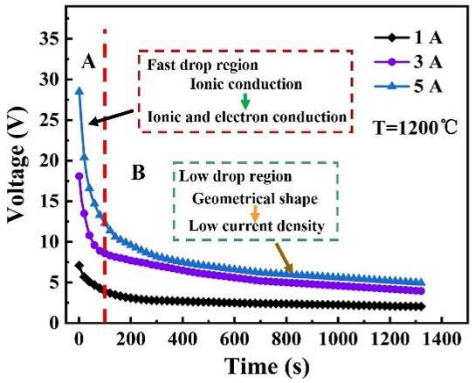

Figure 8. Voltage as a function of deformation time for different electrical currents at 1200 °C.

For example, by applying the electrical current of 5 A (blue curve), the voltage decreased from 28.10 V to 5.09 V. The decreasing of voltage can be divided into two stages: fast drop (before 100 seconds) and slow drop (after 100 seconds). For fast drop section, there was only slight change in the geometrical shape of the specimen when the voltage decreased rapidly. This remarkable drop of voltages indicated that the electrical conductivity may be changed during the deformation. Jane and co-workers demonstrated [33] that this variation of the electrical properties in 3Y-TZP was attributed to the electrochemical reduction reaction induced by the electrical current in oxygen-lean atmosphere. Chen et al. [20]also discovered that the conductivity of 3YSZ in an oxygen-lean atmosphere can be increased when the electric current was applied. They believed that the electrochemical reduction reaction induced by the electric current led to a transition in partial 3YSZ from the ionic conductor into the electron conductor, and further increased the conductivity. As reported by Narayan [38], the

free electron from electrodes were always captured by the extra oxygen vacancies during the electrochemical reduction reaction . As the oxygen vacancies were high enough, these electrons can cause electron conduction as a result of the higher mobility of the electrons. More recently, in Ni-doped MgO, the formation of Ni_0 defects as a result of field treatment produced interesting electrical property modification [39]. In addition, the applied electric fields, work by Yoshida [36], the almost unchanged as the deformation proceeded in air. Therefore, this exaggerated variation of the voltage with deformation time indirectly demonstrated the existence of the electrochemical reduction reaction. For the slow drop section, the decrease of the voltage may be due to the decrease of the current density and height caused by the change of the geometrical shape.

As mentioned above, an electrochemical reduction reaction can be induced in 3Y-TZP during the deformation while the electric current was applied in oxygen-lean atmosphere, which produced the extra oxygen vacancies during the deformation. Such extra oxygen vacancies can promote the cation diffusion of 3Y-TZP, and further decreased the apparent activation energy of the superplastic deformation. Furthermore, some studies demonstrated that the migration energy of the cations in $ZrO_{2-\delta}$ was lower than that in ZrO_2, and the diffusion rate of cation ions in the oxygen-deficient oxides increased with the value of δ [31]. Therefore, in oxygen-lean atmosphere, the electrochemical reduction reaction induced by the electric current is favor to the superplastic deformation of 3Y-TZP by enhancing the cation deformation (lattice diffusion converts to grain boundary diffusion).

4. Conclusions

The compression deformation of 3Y-TZP ceramic with different electric currents in oxygen-lean atmosphere were investigated. The results were summarized as follows:

1. The Superplastic deformation of 3Y-TZP was enhanced by the electric current in oxygen-lean atmosphere. With the electric current increased, the flow stress during deformation had a significant decrease.
2. The stress exponent n ranging within 2～3 indicated that the deformation was dominated by grain boundary sliding. The cation diffusion in3Y-TZP was promoted by the electric current during the deformation. For 0 A, the deformation mechanism was grain boundary sliding accompanied by the lattice diffusion. Upon applying the electric current, it was grain boundary sliding accompanied by the grain boundary diffusion.
3. The grain growth and variation of electrical property in 3Y-TZP indicated that an electrochemical reduction reaction induced by the electric current during the deformation. And the extra oxygen vacancies were generated by this reaction, which can apparently enhance the cation mobility. The enhanced cation diffusion in 3Y-TZP decreased the apparent activation energy Q of the deformation from 465 kJ mol^{-1} to 315 kJ mol^{-1}, resulting in a transition of the diffusion mechanism from the lattice diffusion to the grain boundary diffusion.

Author Contributions: K.W.: Methodology, Data Curation, Conceptualization and Writing—Original Draft Preparation. Y.Z.: Resources and Visualization. G.C.: Methodology and Data curation. X.F.: Data curation and Investigation. W.Z.: Resources, Conceptualization, Supervision, and Writing—Reviewing and Editing. All authors have read and agreed to the published version of the manuscript.

Funding: This work was financial supported by the National Natural Science Foundation of China [grant numbers: U1908229, 52075073], and also supported by the Scientific and technological research projects in Liaoning province [grant number 2021JH1/10400076].

Institutional Review Board Statement: Not applicable.

Informed Consent Statement: Not applicable.

Data Availability Statement: Not applicable.

Conflicts of Interest: The authors declare that they have no known competing financial interests or personal relationships that could have appeared to influence the work reported in this paper.

References

1. Wakai, F.; Kondo, N.; Shinoda, Y. Ceramics Superplasticity. *Curr. Opin. Solid State Mater. Sci.* **1999**, *4*, 461–465, doi:10.1016/S1359-0286(99)00053-4.

2. Chokshi, A.H. A Comparative Examination of Superplastic Flow and Fracture in Metals and Ceramics. *Mater. Sci. Eng. A* **1997**, *234–236*, 986–990, doi:10.1016/S0921-5093(97)00355-9.
3. Wakai, F.; Kodama, Y.; Sakaguchi, S.; Murayama, N.; Izaki, K.; Niihara, K. A Superplastic Covalent Crystal Composite. *Nature* **1990**, *344*, 421–423, doi:10.1038/344421a0.
4. Zapata-Solvas, E.; Gómez-García, D.; García-Gañán, C.; Domínguez-Rodríguez, A. High Temperature Creep Behaviour of 4mol% Yttria Tetragonal Zirconia Polycrystals (4-YTZP) with Grain Sizes between 0.38 and 1.15μm. *J. Eur. Ceram. Soc.* **2007**, *27*, 3325–3329, doi:10.1016/j.jeurceramsoc.2007.02.183.
5. Hiraga, K.; Kim, B.-N.; Morita, K.; Yoshida, H.; Suzuki, T.S.; Sakka, Y. High-Strain-Rate Superplasticity in Oxide Ceramics. *Sci. Technol. Adv. Mater.* **2007**, *8*, 578–587, doi:10.1016/j.stam.2007.09.006.
6. Winnubst, A.J.A.; Boutz, M.M.R. Superplastic Deep Drawing of Tetragonal Zirconia Ceramics at 1160°C. *J. Eur. Ceram. Soc.* **1998**, *18*, 2101–2106, doi:10.1016/S0955-2219(98)00144-7.
7. Nieh, T.G.; Wadsworth, J.; Sherby, O.D. Superplasticity in Metals and Ceramics. *Camb. Univ. Press* **1997**, doi:10.1017/CBO9780511525230.
8. Wakai, F.; Nagano, T. Effects of Solute Ion and Grain Size on Superplasticity of ZrO2 Polycrystals. *J. Mater. Sci.* **1991**, *26*, 241–247, doi:10.1007/BF00576058.
9. Morita, K.; Hiraga, K.; Kim, B.N. High-Strain-Rate Superplastic Flow in Tetragonal ZrO2 Polycrystal Enhanced by the Dispersion of 30 Vol.% MgAl2O4 Spinel Particles. *Acta Mater.* **2007**, *55*, 4517–4526, doi:10.1016/j.actamat.2007.04.016.
10. Yoshida, H.; Morita, K.; Kim, B.-N.; Hiraga, K.; Yamamoto, T. Doping Amount and Temperature Dependence of Superplastic Flow in Tetragonal ZrO2 Polycrystal Doped with TiO2 and/or GeO2. *Acta Mater.* **2009**, *57*, 3029–3038, doi:10.1016/j.actamat.2009.03.009.
11. Conrad, H. Electroplasticity in Metals and Ceramics. *Mater. Sci. Eng. A* **2000**, *287*, 276–287, doi:10.1016/S0921-5093(00)00786-3.
12. Conrad, H.; Yang, D. Influence of an Applied DC Electric Field on the Plastic Deformation Kinetics of Oxide Ceramics. *Philos. Mag.* **2010**, *90*, 1141–1157, doi:10.1080/14786430903304137.
13. Yang, D.; Conrad, H. Influence of an Electric Field on the Superplastic Deformation of 3Y-TZP. *Scr. Mater.* **1997**, *36*, 1431–1435, doi:10.1016/S1359-6462(97)00045-6.
14. Conrad, H.; Yang, D.; Becher, P. Plastic Deformation of Ultrafine-Grained 2.5Y-TZP Exposed to a Dc Electric Field with an Air Gap. *Mater. Sci. Eng. A* **2008**, *496*, 9–13, doi:10.1016/j.msea.2008.07.012.
15. Conrad, H.; Yang, D. Effect of an Alternating Current Electric Field on the Plastic Deformation of Ultrafine-Grained 3Y-TZP at 1400 °C and 1500 °C. *Metall. Mater. Trans. A* **2008**, *39*, 272–278, doi:10.1007/s11661-007-9396-y.
16. Conrad, H.; Yang, D. Effect of DC Electric Field on the Tensile Deformation of Ultrafine-Grained 3Y-TZP at 1450–1600°C. *Acta Mater.* **2007**, *55*, 6789–6797, doi:10.1016/j.actamat.2007.08.032.
17. Francis, J.S.C.; Raj, R. Influence of the Field and the Current Limit on Flash Sintering at Isothermal Furnace Temperatures. *J. Am. Ceram. Soc.* **2013**, *96*, 2754–2758, doi:10.1111/jace.12472.
18. Zhang, Y.; Luo, J. Promoting the Flash Sintering of ZnO in Reduced Atmospheres to Achieve Nearly Full Densities at Furnace Temperatures of <120°C. *Scr. Mater.* **2015**, *106*, 26–29, doi:10.1016/j.scriptamat.2015.04.027.
19. Hulbert, D.M.; Jiang, D.; Kuntz, J.D.; Kodera, Y.; Mukherjee, A.K. A Low-Temperature High-Strain-Rate Formable Nanocrystalline Superplastic Ceramic. *Scr. Mater.* **2007**, *56*, 1103–1106, doi:10.1016/j.scriptamat.2007.02.003.
20. Dong, Y.; Wang, H.; Chen, I.-W. Electrical and Hydrogen Reduction Enhances Kinetics in Doped Zirconia and Ceria: I. Grain Growth Study. *J. Am. Ceram. Soc.* **2016**, doi:10.1111/jace.14615.
21. Dong, Y.; Chen, I. Electrical and Hydrogen Reduction Enhances Kinetics in Doped Zirconia and Ceria: II . Mapping Electrode Polarization and Vacancy Condensation in YSZ. *J. Am. Ceram. Soc.* **2018**, *101*, 1058–1073, doi:10.1111/jace.15274.
22. Birkby, I.; Stevens, R. Applications of Zirconia Ceramics. *Key Eng. Mater.* **1996**, *122–124*, 527–552, doi:10.4028/www.scientific.net/kem.122-124.527.
23. Wakai, F.; Nagono, T. The Role of Interface-Controlled Diffusion Creep on Superplasticity of Yttria-Stabilized Tetragonal ZrO2 Polycrystals. *J. Mater. Sci. Lett.* **1988**, *7*, 607–609, doi:10.1007/BF01730309.
24. Owen, D.M.; Chokshi, A.H. The High Temperature Mechanical Characteristics of Superplastic 3 Mol% Yttria Stabilized Zirconia. *Acta Mater.* **1998**, *46*, 667–679, doi:10.1016/S1359-6454(97)00251-6.
25. Hines, J.A.; Ikuhara, Y.; Chokshi, A.H.; Sakuma, T. The Influence of Trace Impurities on the Mechanical Characteristics of a Superplastic 2mol% Yttria Stabilized Zirconia. *Acta Mater.* **1998**, *46*, 5557–5568, doi:10.1016/S1359-6454(98)00171-2.
26. Yang, D.; Conrad, H. Retardation of Grain Growth and Cavitation by an Electric Field during Superplastic Deformation of Ultrafine-Grained 3Y-TZP at 1,450–1,600 °C. *J. Mater. Sci.* **2008**, *43*, 4475–4482, doi:10.1007/s10853-008-2653-7.
27. Raj, R. Joule Heating during Flash-Sintering. *J. Eur. Ceram. Soc.* **2012**, *32*, 2293–2301, doi:10.1016/j.jeurceramsoc.2012.02.030.

28. Swaroop, S.; Kilo, M.; Argirusis, C.; Borchardt, G.; Chokshi, A.H. Lattice and Grain Boundary Diffusion of Cations in 3YTZ Analyzed Using SIMS. *Acta Mater.* **2005**, *53*, 4975–4985, doi:10.1016/j.actamat.2005.05.031.
29. Yoshida, H.; Morita, K.; Kim, B.N.; Hiraga, K.; Yamamoto, T. Doping Amount and Temperature Dependence of Superplastic Flow in Tetragonal ZrO2 Polycrystal Doped with TiO2 and/or GeO2. *Acta Mater.* **2009**, *57*, 3029–3038, doi:10.1016/j.actamat.2009.03.009.
30. Swaroop, S.; Kilo, M.; Argirusis, C.; Borchardt, G.; Chokshi, A.H. Lattice and Grain Boundary Diffusion of Cations in 3YTZ Analyzed Using SIMS. *Acta Mater.* **2005**, *53*, 4975–4985, doi:10.1016/j.actamat.2005.05.031.
31. Chen, P.L.; Chen, I.W. Role of Defect Interaction in Boundary Mobility and Cation Diffusivity of CeO2. *J. Am. Ceram. Soc.* **1994**, *77*, 2289–2297, doi:10.1111/j.1151-2916.1994.tb04596.x.
32. Liu, D.; Cao, Y.; Liu, J.; Gao, Y.; Wang, Y. Effect of Oxygen Partial Pressure on Temperature for Onset of Flash Sintering 3YSZ. *J. Eur. Ceram. Soc.* **2018**, *38*, 817–820, doi:10.1016/j.jeurceramsoc.2017.09.009.
33. Janek, J.; Korte, C. Electrochemical Blackening of Yttria-Stabilized Zirconia – Morphological Instability of the Moving Reaction Front. *Solid State Ion.* **1999**, *116*, 181–195, doi:10.1016/S0167-2738(98)00415-9.
34. Biesuz, M.; Pinter, L.; Saunders, T.; Reece, M.; Binner, J.; Sglavo, V.M.; Grasso, S. Investigation of Electrochemical, Optical and Thermal Effects during Flash Sintering of 8YSZ. *Materials* **2018**, *11*, 1214, doi:10.3390/ma11071214.
35. Moghadam, F.K.; Yamashita, T.; Stevenson, D.A. Characterization of the Current-Blackening Phenomena in Scandia Stabilized Zirconia Using Transmission Electron Microscopy. *J. Mater. Sci.* **1983**, *18*, 2255–2259, doi:10.1007/BF00541827.
36. Yoshida, H.; Sasaki, Y. Low Temperature and High Strain Rate Superplastic Flow in Structural Ceramics Induced by Strong Electric-Field. *Scr. Mater.* **2018**, *146*, 173–177, doi:10.1016/j.scriptamat.2017.11.042.
37. Sinhamahapatra, A.; Jeon, J.P.; Kang, J.; Han, B.; Yu, J.S. Oxygen-Deficient Zirconia (ZrO2x): A New Material for Solar Light Absorption. *Sci. Rep.* **2016**, *6*, 27218, doi:10.1038/srep27218.
38. Narayan, J. A New Mechanism for Field-Assisted Processing and Flash Sintering of Materials. *Scr. Mater.* **2013**, *69*, 107–111, doi:10.1016/j.scriptamat.2013.02.020.
39. Controlled P-Type to n-Type Conductivity Transformation in NiO Thin Films by Ultraviolet-Laser Irradiation | Journal of Applied Physics | AIP Publishing Available online: https://pubs.aip.org/aip/jap/article/111/1/013706/925879/Controlled-p-type-to-n-type-conductivity (accessed on 23 May 2023).